Nuclear Engineering and Design 428 (2024) 113559

Contents lists available at ScienceDirect

Nuclear Engineering and Design

journal homepage: www.elsevier.com/locate/nucengdes

# Euler–Euler modeling of turbulent annular regime

Kshitij Neroorkar [a,*], Mohit P. Tandon [b], Dimitrios Papoulias [c]

[a] Siemens Industry Software India (Private) Limited, Bangalore, 560048, India
[b] Siemens Industry Software India (Private) Limited, Gurgaon, 122002, India
[c] Siemens Industries Software Computational Dynamics Ltd., London, W67HA, UK

ARTICLE INFO

*Keywords:*
Annular flows
Liquid film
Boiling water reactor
Two-fluid model
Turbulent film

ABSTRACT

Euler–Euler methods are one of the many approaches available in literature for modeling droplet-laden flows. These models consider both the gas and droplet phases as inter-penetrating continua, thereby separate sets of transport equations are solved for these phases. The current work focuses on modeling of thin liquid films on solid surfaces in the context of the two-fluid approach to multiphase simulation. In majority of the literature, liquid films are modeled using a 2D Laminar approximation with a parabolic profile for the velocity across the film. However, a number of industrial applications demonstrate a turbulent behavior of the film which would affect the effective viscosity and thereby the thickness of the film. In the current work, a turbulent model for liquid films is proposed based on the Universal Velocity Profile. Additional models are employed to capture the deposition of droplets onto solid surface and stripping off of droplets from the film due to surface waves. The liquid film model is validated on experimental data from available literature. Finally, the newly implemented turbulent film model is applied to study the flow over a fuel rod assembly in a Boiling Water Reactor.

## 1. Introduction

Multiphase flows occur in many different types of industrial equipment like boilers, condensers, nuclear reactor cores, etc and are generally characterized by four different regimes, namely bubble flow, plug flow, churn flow, and annular flow (Govan, 1990). Annular flows are a regime of multiphase flows which comprise of a gas flowing in most of the cross section of the geometry, and a thin film of liquid flowing along the walls along with some droplets in gas core. Annular regimes occur for very high superficial gas velocities, and in most cases, are characterized by waves at the liquid–gas interface which cause small drops of liquid to strip off from the film. Simultaneously, the drops dispersed in the gas may hit the walls and deposit onto the film leading to a continuous exchange of mass across the liquid–gas interface.

Such annular flows with liquid films appear in many industrial applications like Boiling Water Reactors (BWR), internal combustion engines, building drainage systems (BDS), refrigerant flows in evaporators, etc, and the modeling of films is extremely important for design and analysis of these systems. A lot of work is being done recently to improve the current understanding of two-phase flows in BDS post COVID-19 pandemic (Xue et al., 2022). In nuclear power plants, the annular flow observed in the BWR is crucial to the efficiency of the power plant. In a BWR, the fuel rods are cooled by evaporation of the liquid film flowing on the rod surface. However, in some cases, the liquid film is no longer able to efficiently wet the wall so that the heat transfer from the fuel rod surface is greatly diminished, and this condition is known as dryout. The possibility of leakage, bending or in the worst case melting of the fuel elements due to the enhanced temperatures have led to a lot of interest in modeling the annular flow regime in the nuclear industry from the perspective of safety (Hewitt and Hall-Taylor, 1970).

Once the dryout occurs, the rewetting of the dry spot is difficult and needs up to ten times the liquid mass flow rate compared to the moment just before the dryout (Hewitt and Lacey, 1965; McPherson, 1970). If the waves of liquid film are sufficiently frequent, a dryout may occur for a short instance as the waves of liquid carried by the gas shear easily rewet and cool the rod (Mori and Fukano, 2003; Damsohn, 2011). This is why understanding the transient nature of liquid film and its dryout is crucial.

A lot of research has been done to better understand mechanisms that govern dryout and are related to accurate prediction of its occurrence. The dryout prediction relies on accurate local value of liquid film flow rate. It is famously referred that there is a "triangular relationship" between film thickness, interfacial shear stress and liquid film flow rate implying that if two of these are known, the third can also be determined (Hewitt and Hall-Taylor, 1970) though the relationship was developed without considering gravity. Phenomenological modeling

* Corresponding author.
*E-mail addresses:* kshitij.neroorkar@siemens.com (K. Neroorkar), mohit.tandon@siemens.com (M.P. Tandon).

https://doi.org/10.1016/j.nucengdes.2024.113559
Received 5 March 2024; Received in revised form 1 August 2024; Accepted 20 August 2024
Available online 27 August 2024

**Nomenclature**

| | |
|---|---|
| $k$ | Deposition mass transfer coefficient/ deposition velocity |
| $C$ | Mean Droplet concentration |
| $C^*$ | Dimensionless concentration = $C/\rho_G$ |
| $C_1, C_2, C_3, C_4, C_5, C_{0\infty}$ | modeling constants |
| $D$ | Diameter |
| $E$ | Entrainment fraction |
| $K$ | Turbulent kinetic energy |
| $La$ | Lagrangian integral time scale |
| $P$ | Pressure |
| $Re$ | Reynolds number |
| $S_c$ | Source/Sink in Continuity equation |
| $S_m$ | Source/Sink in Momentum equation |
| $T$ | Relaxation time |
| $V_e$ | Volume of film stripped |
| $We$ | Weber number |
| $\dot{m}$ | Mass flow rate |
| $\dot{m}_{dep}$ | Deposition rate per unit wall area |
| $f_b$ | Body force vector |
| $f_{intP}$ | interphase force between the Continuous and Dispersed phases |
| $g$ | Acceleration due to gravity |
| $h$ | Film thickness |
| $h_a$ | Film thickness to be stripped/ amplitude of surface wave |
| $h_{pm}$ | Film thickness corresponding to the intersection between two parts of universal velocity profile |
| $k^*$ | Dimensionless mass transfer coefficient = $k\sqrt{\frac{\rho_G D_p}{\sigma}}$ |
| $l$ | Width of the film section |
| $n$ | Normal into the film |
| $v$ | Velocity |
| $v'$ | RMS fluctuating velocity |
| $v^+$ | Non dimensional velocity = $\frac{v}{v_*}$ |
| $v_*$ | Friction velocity |
| $x$ | Coordinate in flow direction |
| $y$ | Wall normal coordinate |
| $y^+$ | Non dimensional wall normal coordinate = $\frac{yv_*}{\nu_f}$ |

**Greek Letters**

| | |
|---|---|
| $\alpha$ | Volume fraction |
| $\beta$ | Number of spherical droplets created by stripping of one film ligament of height $h_a$ and width l |
| $\delta$ | Film thickness |
| $\epsilon$ | Turbulent dissipation rate |
| $\gamma$ | Thickness of laminar layer |
| $\kappa$ | Wave number |
| $\kappa_{VK}$ | Von Kármán constant = 0.4 |
| $\lambda$ | Wavelength |
| $\nu$ | Kinematic viscosity |
| $\omega$ | Wave frequency |
| $\phi$ | Fraction of droplets hitting the wall/ deposition efficiency |
| $\rho$ | Density |
| $\sigma$ | Surface tension |
| $\tau$ | Viscous stress tensor |

**Subscripts**

| | |
|---|---|
| $d$ | Droplet |
| $dep$ | Deposition |
| $F$ | Fluid surrounding film |
| $f$ | Film |
| $G$ | Gas |
| $i$ | Different phases in the domain, viz Continuous/Dispersed |
| $in$ | Inlet of test section |
| $int$ | Interface between film and surrounding fluid |
| $L$ | Liquid |
| $out$ | Outlet of test section |
| $p$ | Pipe |
| $s$ | Superficial quantity |
| $w$ | Wall |

of liquid film was proposed based on rate of evaporation, droplet entrainment and droplet deposition (Hewitt and Govan, 1990; Okawa et al., 2003). However, such models adopt certain assumptions on the location and shape of the liquid film - gas core interface.

Although it is possible to resolve the liquid film - gas core interface rigorously using Interface Tracking methods as they are free from any assumptions, they are computationally exhaustive and so not practical for industrial applications. Therefore, it becomes necessary that mechanistic models are developed for liquid film flow, and for convenience following phenomena are considered separately with appropriate closure terms where required: (a) gas core flow (b) liquid film flow and (c) droplet exchange between liquid film and gas core through evaporation, droplet deposition and droplet entrainment. Such approaches employ proper boundary conditions at the interface for conservation of mass, momentum, and energy. Such approaches were deveoped by many authors (Bai and Gosman, 1996; Meredith et al., 2011; Li and Anglart, 2015; Anglart et al., 2018) where gas core could be modeled using either the Euler–Euler or Euler-Lagrangian techniques and liquid film is modeled using two-dimensional model developed by integrating the transport equations of the liquid film in the wall-normal direction to obtain two-dimensional equations. In this study, we build on above approaches through the use of Euler–Euler methodology for the gas core. However, we restrict our study to adiabatic flows excluding evaporation of liquid into gas-core since droplet deposition and droplet entrainment happen under adiabatic conditions as well and it would be convenient to validate their modeling without the effects of heat transfer.

In general, majority of the literature focuses on laminar modeling for the liquid films due to its low thickness. However, in many practical applications liquid film entrainment is due to disturbance waves which are also referred as “roll waves” and are bigger sized waves that move at a higher velocity than the smaller regular waves also referred as “ripple waves”. These roll waves are of a very turbulent nature (Damsohn, 2011). Turbulence increases the effective viscosity of the liquid film and thereby makes the film less stable. Joseph et al. (1996) proposed an effective viscosity criterion which demonstrated that annular flow is stable when the fluid having the higher effective viscosity occupies the core region and the fluid with lower effective viscosity is in the annulus. Many authors have attempted to apply theories of single phase turbulent flow to liquid films in annular systems, and have been able to satisfactorily predict experimental data for film thickness and film

flow rate (Hewitt and Hall-Taylor, 1970; Calvert and Williams, 1955; Dukler, 1959).

In the current work, a turbulence model for liquid films is proposed which uses the Universal Velocity Profile. The purpose of this paper is to demonstrate a computational tool which is capable of predicting liquid film behavior in various types of industrial applications. To this end, the new model is implemented within the commercial code Simcenter StarCCM+ and is applied for simulations on a fuel assembly of a Boiling Water Reactors.

## 2. Past work

Vasallo (1999) performed near-wall measurements of the liquid mean and fluctuating velocities in a liquid film in vertical air–water annular flow using the Hot Film Anemometry technique. Their data showed that for annular flow with thin films, the law-of-the-wall developed for single phase flows could be used to predict the near wall behavior. However, if the film thickness is higher and the film is highly turbulent, the law-of-the-wall could still predict the trends, but the value of the constants needed to be adjusted. Ashwood et al. (2015) demonstrated that the universal velocity profile shows good agreement with their velocity data close to the wall, but starts deviating in the log region and needs to be modified so as to accommodate the reduction in turbulence mixing close to the film-gas interface. Cioncolini et al. (2009) also showed that using the universal velocity profile gives a reasonable estimate of the average film thickness.

An important aspect is deciding whether turbulence is important for the flow conditions which are prevalent in a given application. Friedman and Miller (1941) analyzed falling annular films in vertical pipes and indicated that liquid films running downward with a stationary air core become turbulent at Reynolds numbers of 1000. However, Calvert and Williams (1955) postulate that this method does not account for the momentum transfer between the film and the air. They used a criteria to determine whether the film is turbulent by using the concept that the thickness of the laminar layer $\gamma$ to the pipe diameter for a single phase pipe flow is a function of Reynolds number and the friction factor. By analogy, the criteria for film turbulence is decided from the ratio of $\gamma$ to the film thickness. A critical value of this ratio is determined from the data of Friedman and Miller (1941) as,

$$\gamma/\delta = 0.425 \tag{1}$$

This critical ratio marks the point of abrupt change from turbulent to laminar flow. If its value is larger than 0.425, the flow pattern will be laminar. The above criteria essentially means that the film will be entirely laminar at a point where roughly half its thickness would flow by a laminar mechanism even if the flow were turbulent. This criterion was applied to vertical upward annular flow of water and it was concluded that these flows are predominantly turbulent.

Owing to the complexity of the interaction between the liquid film and the gas in the core, a number of closure relationships are required to describe the transfer of mass, momentum, and energy between the film and the core. One of the phenomena which are modeled is the deposition of droplets on the solid surface. Young and Leeming (1997) showed that based on the inertia of the droplets, the mechanism of droplet deposition can be differentiated into three regimes. For very light particles, the motion to the wall takes place through turbulent diffusion in the core of the channel and Brownian diffusion in a very thin layer adjacent to the wall. For slightly larger particles, the motion is mainly governed by the turbulence. Finally, large particles are unaffected by turbulence and impact the wall on account of their own inertia.

The equation which is widely used in literature for calculation of deposition rate per unit wall area is,

$$\dot{m}_{dep} = kC \tag{2}$$

A number of correlations are available in literature for calculating $k$, (Govan, 1990; Okawa et al., 2003; Utsuno and Kaminaga, 1998; Paleev and Filippovich, 1966; Hewitt and Hall-Taylor, 1970). However, in all cases, these correlations are tuned for certain types of experiments. Caraghiaur (2012) proposed a more mechanistic model which is dependent on local concentration of drops and the droplet fluctuating velocity. Based on analysis of existing experimental data by Caraghiaur and Anglart (2008), it was concluded that the drops in annular two-phase flow, based on the Sauter mean diameter, fall in the inertia-moderated regime. So, Caraghiaur (2012) formulated a model to capture the behavior of droplets lying in this regime. As part of the current work, the model of Caraghaiur is used for modeling the deposition process.

Another critical phenomenon which requires to be modeled is the entrainment of the droplets from the film into the core. As the liquid film flows along the surface, waves are generated due to its interaction with the gas flowing over it, and can lead to entraiment of droplets from the film into the gas (Anglart, 2012). As the gas phase velocity adjacent to the fluid film is increased, the amplitude and irregularity of the waves become pronounced, and eventually the amplitudes of these so called roll waves become large enough that the entrainment starts occurring from the film due to shearing off of the wave crests (Ishii and Mishima, 1989). Sawant et al. (2009) proposed a schematic of the entrainment fraction with respect to the modified Weber number which can be divided into three regions, viz. a Weber number dependent region, a transition region, and a liquid phase Reynolds number dependent region. Based on this schematic curve, Sawant et al. (2009) proposed empirical correlations for the entrainment fraction, and the limiting entrainment fraction which were applicable for vertical upward annular flows. Al-sarkhi and Sarica (2013) also developed a correlation for the entrainement fraction based on the curve proposed by Sawant et al. (2009). Their formulation was found to predict the entrainment fraction better than the model of Sawant et al. (2009) for cases with low liquid Reynolds numbers.

Many other correlations exist which are based on different dimensionless numbers, for example Ishii and Mishima (1989) proposed a correlation for the fully developed entrainment fraction as a function of the dimensionless hydraulic diameter, the dimensionless gas flux, and the liquid Reynolds number. Sawant et al. (2009) noted that the upper limit of the entrainment fraction was observed to be much less than the value of 1 assumed by Ishii and Mishima (1989) even in experiments performed at high gas velocities. Cioncolini and Thome (2010) tested 9 different empirical correlations for the entrainment fraction on a large database of experimental data and found that the model of Sawant et al. (2009) and Oliemans et al. (1986) reproduced the data the best. The sigmoid trend of the curve proposed by Sawant et al. (2009) is similar to the one obtained by Cioncolini and Thome (2010) by plotting the available experimental data for entrainment fraction versus the core flow Weber number. Cioncolini and Thome (2010) also proposed a new correlation for the entrainment fraction as a function of the core flow Weber number which was solved using an iterative procedure and was found to reproduce the database of experiments better than the tested models.

There have also been a number of attempts to model this phenomenon using mechanistic models with relationships for the wavelength and velocities of the instabilities. For example, Liu and Bai (2017) and Holowach (2002) used the interfacial stability analysis discussed by Hewitt and Hall-Taylor (1970) to obtain the critical wavelength of disturbance wave for the condition that the wave amplitude does not increase. The entrained volume is then obtained by performing a force balance on the wave crests. In the current work, the model developed by Foucart (1998) is employed which is based on the linear instability theory and is explained in more details in the following section.

## 3. Formulation

### 3.1. Turbulent film model

The film flow model assumes that the film is 2D, which allows for a simplified solution procedure for the film flow. The continuity equation is solved for the film thickness ($h_f$) and is given below,

$$\frac{\partial}{\partial t}\int_V \rho_f dV + \int_A \rho_f v_f \cdot dA = \int_V \frac{S_{cf}}{h_f} dV \tag{3}$$

The momentum equation is solved for the average velocity of the film ($v_f$), and is given below,

$$\frac{\partial}{\partial t}\int_V \rho_f v_f dV + \int_A \rho_f v_f v_f \cdot dA = \int_A \tau_f \cdot dA - \int_A P_f dA + \int_V (f_{bf} + \frac{S_{mf}}{h_f}) dV \tag{4}$$

At the interface of the film, the following conditions are enforced,

$$v_f|_{int} = v_F|_{int} \tag{5}$$

$$(\tau_f . dA + P_f . dA)|_{int} = (\tau_F . dA + P_F . dA)|_{int} \tag{6}$$

As mentioned previously, in many practical applications of annular two-phase flow, the Reynolds numbers in the liquid film are in the turbulent range by analogy with single phase flows, and it is found that laminar flow based film models are unable to accurately predict film behavior (Hewitt and Hall-Taylor, 1970).

In the turbulent film model, we use the widely accepted Universal Velocity Profile to calculate the flow variables (Neroorkar and Tandon, 2022). The non-dimensional velocity, $v^+$ is calculated as,

$$v^+ = \begin{cases} y^+ & 0 < y < h_{pm} \\ \frac{1}{\kappa_{VK}} ln(y^+) + C_1 & h_{pm} < y < h \end{cases} \tag{7}$$

The constant $C_1$ is taken to be 5.5. The friction velocity for the film ($v_{*f}$) is calculated as,

$$v_{*f} = \sqrt{\frac{\tau_w}{\rho_f}} \tag{8}$$

The following solution procedure is followed to obtain the flow variables of film surface velocity and turbulent wall shear stress:

1. In order to compute $h_{pm}$, first an initial value is assumed and then the theoretical intersection of the two parts of Eq. (7) is computed iteratively using the Newton–Raphson method.
2. From the momentum equation, Eq. (4), we have the solution of the average film velocity $v_f$. Our next step in the turbulent film model procedure is to calculate the friction velocity $v_*$. For this, we modify the Eq. (7) into an equation for average velocity by integrating as,

   $$v_f = \frac{v_*}{h}\int_0^h v dh \tag{9}$$

   This gives us an equation in which the only unknown is $v_*$. Using the value of film thickness obtained from the continuity equation, we solve Eq. (9) using Newton–Raphson to obtain the friction velocity.
3. The friction velocity is then used to calculate the wall shear stress from Eq. (8).
4. Finally, the surface velocity of the film is obtained by substituting the film thickness into Eq. (7).

In contrast to the above proposed turbulent model, the laminar liquid film model assumes a parabolic velocity distribution in the flow normal direction. The parabolic profile is derived by first assuming the velocity across the film to be a parabolic function of the wall normal coordinate.

$$v = C_2 y^2 + C_3 y + C_4 \tag{10}$$

In order to find the 3 coefficients, we apply the following 3 conditions

1. Velocity condition at the wall, i.e. $y$ =0.
2. Shear stress at the interface, i.e. at y=h,

   $$\frac{\partial v}{\partial y} = \frac{\tau_f|_{int}}{h_f} \tag{11}$$

3. Average Velocity $v_f = 1/h \int_0^h v dh$

This gives the coefficients as functions of $v_f$ which is obtained from the solution of the film momentum equation, and $\tau_f|_{int}$ which comes from the interface condition Eq. (6).

### 3.2. Film-droplet exchange models

The following section provides the formulations of the various sub-models which are employed to capture the mass and momentum transfers between the film and the gas-core.

#### 3.2.1. Film deposition model

The drop deposition rate per unit interfacial area of the liquid film as defined by Caraghiaur (2012) is as follows:

$$m_{dep} = \phi \sqrt{\frac{2}{\pi}} v'_d * \alpha_d \rho_L \tag{12}$$

It can be observed that the term $\alpha_d \rho_L$ is the droplet concentration. The droplet's RMS fluctuating velocity ($v'_d$) is calculated using the relation of Tchen (Hinze, 1975).

$$\frac{v'^2_G}{v'^2_d} = 1 + \frac{T_d}{L_{aG}} \tag{13}$$

The relaxation time $T_d$ is a measure of the inertia of the droplet which is calculated as,

$$T_d = \frac{T_{d0}}{\psi(Re_P)} \tag{14}$$

Where,

$$\psi(Re_d) = \begin{cases} 1 + 0.15 Re_d^{0.687} & at\, Re_d <= 10^3 \\ 0.11 Re_d/6 & at\, Re_d > 10^3 \end{cases} \tag{15}$$

$$Re_d = \frac{D_d |v_G - v_d|}{\nu_G} \tag{16}$$

And,

$$T_{d0} = \frac{\rho_d d_d^2}{18 \rho_G \nu_G} \tag{17}$$

The variable $L_{aG}$ represents the Lagrangian integral time scale of the gas following the path of an inertial drop. The equation of Zaichik et al. (2008) gives $L_{aG}$ as,

$$L_{aG} = \frac{4}{3}\frac{K_G}{C_0 \epsilon_G} \tag{18}$$

$$C_0 = \frac{C_{0\infty} Re_\lambda}{Re_\lambda + C_5} \tag{19}$$

$$Re_\lambda = \sqrt{\frac{15 v'^4_G}{\epsilon_G \nu_G}} \tag{20}$$

Where $C_{0\infty} = 7.0$ and $C_5 = 32.0$.

#### 3.2.2. Entrainment model

For modeling the entrainment of droplets from the film, we start with the equation for waves on the surface of a film presented in Camatte et al. (1993). Camatte et al. used the linear instability theory to derive a dispersion equation for a instability of a liquid sheet in an Air-blast atomizer. Foucart (1998) modified this equation by adding the effect of gravity to arrive at the following,

$$\rho_G(\omega - \kappa v_G)^2 \frac{1}{tan(\kappa h)} - \rho_f(\omega - \kappa v_f)^2 = \sigma_f \kappa^3 + \rho_f g \cdot n\kappa \tag{21}$$

Where, the wave number ($\kappa$) is defined as $2\pi/\lambda$. On solving this equation, an equation is obtained for the wave frequency as,

$$\omega = \kappa \frac{\rho_f v_f + \rho_G v_G}{\rho_f + \rho_G} + i\kappa(v_G - v_f)\frac{\sqrt{(1 - We_{int})\rho_f \rho_G}}{\rho_f + \rho_G} \tag{22}$$

Where, the Weber number at the film-gas interface is defined,

$$We_{int} = \frac{1}{(v_G - v_f)^2}\left(\frac{1}{\rho_G} + \frac{1}{\rho_f}\right)\left(\sigma\kappa + \frac{\lambda \rho_f g \cdot n}{2\pi}\right) \tag{23}$$

It is assumed that the film strips off when the instability is maximum, which would be achieved when the imaginary part of Eq (22) is maximum. This corresponds to a value of the Weber number equal to 2/3 (Ledoux, 1993). Substituting for $We_{int} = 2/3$ in Eq. (23), a quadratic equation is obtained in $\lambda$ which can be solved to obtain the following root:

$$\lambda = \frac{2\pi}{\rho_f g \cdot n}\left[\frac{1}{3}\Delta v^2 \rho_G - \sqrt{\frac{1}{3}\rho_G \Delta v^2 - \rho_f g \cdot n\sigma}\right] \tag{24}$$

This wavelength of the most unstable wave provides the criteria for stipping to happen. In order to determine the fraction of the film which would strip off, we start by assuming the surface of the film to have a sinusoidal shape giving the following for the film height:

$$h = h_a\left(sin\frac{2\pi}{\lambda}x + 1\right) \tag{25}$$

If we assume that the surface of the wave between two troughs is stripped off, the volume of the stripped liquid is obtained by integration as follows,

$$V_e = l\int_0^{\lambda} h dh \tag{26}$$

Substituting from Eq. (25), and integrating, we get the volume ($V_e$) as $lh_a\lambda$. If we assume that each of such stripped ligaments breaks up into $\beta$ number of spherical droplets, we get another equation for the volume ejected as

$$V_e = \beta\frac{4}{3}\pi\left(\frac{D_d}{2}\right)^3 \tag{27}$$

The diameter of droplets formed from stripping is determined using the correlation of Maroteaux et al. (2002). Maroteaux et al. assumed an atomization scheme in which each surface wave produces a ligament which breaks into droplets as per the theory of Rayleigh (Lefebvre and McDonell, 2017). This theory provides a droplet diameter as follows:

$$D_d = 3.78\sqrt{\frac{\lambda h_a}{\pi}} \tag{28}$$

Combining Eqs. (26) and (27), and substituting for diameter from Eq. (28) with the assumption that the number of drops formed $\beta = l/\lambda$, we get the following equation for the amplitude of the surface wave,

$$h_a = 0.03877\lambda \tag{29}$$

The amplitude of the surface wave $h_a$ is assumed to be equal to the film height which will be stripped off. By substituting $h_a$ from Eq. (29) and $\lambda$ from Eq. (24) into Eq. (28) the diameter of the stripped droplets is obtained. The volume of the stripped liquid is then calculated by multiplying $h_a$ with the area of the film. This volume of stripped liquid then gets added to the source term of the droplet equation presented in Section 3.2.3.

The above mechanisms are essentially mass exchanges between the film and the droplet phase, and are handled by first calculating the mass lost or gained by the film. In the next step, this mass along with the associated momentum are used as source or sink terms in the droplet and film equations. The droplet equations are presented in the following section. The diameter of the droplets predicted by the stripping/entrainment models can be used as an input to the size distribution models similar to ones presented in Tandon et al. (2013) and Vikhansky and Splawski (2015). Additionally, in the stripping model, we sometimes run into the situation that the amount of mass added to the droplet phase is so large that it can "flood" the computation cell. To prevent this situation from occurring, we perform a conservative numerical redistribution of the source terms in the vicinity of the receiver cell by an approach known as "source smoothing". A model parameter is used to control the number of cell layers over which the redistribution can take place.

#### 3.2.3. Eulerian multi-fluid model description

In the core of the annular flow, an Eulerian Multi-Fluid approach is used to model the flow of gas and droplets. In this method, each phase has its own properties like velocity, temperature, etc. As a result, conservation equations are solved for each phase and additional closure laws are required to model the interactions between the phases.

The continuity equation for each phase "i" (droplet/gas) takes the following form:

$$\frac{\partial \alpha_i \rho_i}{\partial t} + \nabla \cdot \alpha_i \rho_i v_i = S_{ci} \tag{30}$$

And the momentum equation is as follows:

$$\frac{\partial \alpha_i \rho_i v_i}{\partial t} + \nabla \cdot \alpha_i \rho_i v_i v_i = -\alpha_i \nabla P + \alpha_i \rho_i f_{bi} + \nabla \cdot \tau_i + f_{intP} + S_{mi} \tag{31}$$

The impingement and entrainment models presented in the previous sections contribute to the "droplet" equations through $S_{mi}$.

## 4. Results and discussion

In this section, before validating the newly proposed turbulence model, a validation of the different sub-models is presented. In Section 4.1, we include the validation of the individual models, namely, the models for entrainment and deposition. The subsequent section focuses on validation of the proposed turbulence model. Finally, Section 4.3 includes a case of flow over fuel rods in a Boiling Water Reactor.

### 4.1. Base model validation

As was mentioned earlier, drops in annular flow belong to the Inertia-Moderated regime, and the impingement model of Caraghiaur (2012) was developed to model such droplets. Fig. 1 shows the results of the dimensionless deposition velocity versus the relaxation time results obtained from the current work in comparison with the experimental data from Liu and Agarwal (1974). For this validation, a pipe geometry of diameter 31.8 mm was used including an initial section of 1 m length to allow the flow to reach fully developed condition, and after this section, the film was allowed to be formed. A deposition length of 150 mm was used to extract the results which are presented. The gas and liquid mass fluxes were kept constant at 100 $kg/m^2s$ and 5 $kg/m^2s$ respectively. In order to capture the effect of different particle relaxation times, the injected droplet diameter is varied from 3 μm to 80 μm. It can be seen that the model reproduces the behavior in the inertial dominated regime quite well and the trend is captured satisfactorily. The definition of the deposition velocity is deduced from the Eq. (12) by assuming that $\alpha_d \rho_L$ represents the concentration, therefore from Eq. (2), we get that the deposition velocity is equal to:

$$k = \phi\sqrt{\frac{2}{\pi}}v_d' \tag{32}$$

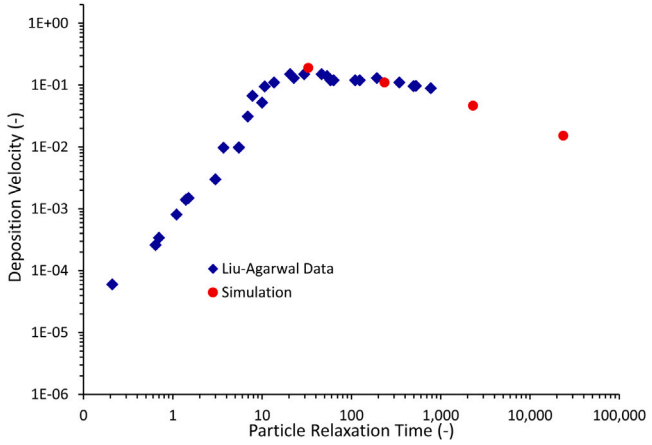


**Fig. 1.** Deposition velocity plotted against the particle relaxation time. Comparison of the simulation results with experimental data of Liu and Agarwal (1974).

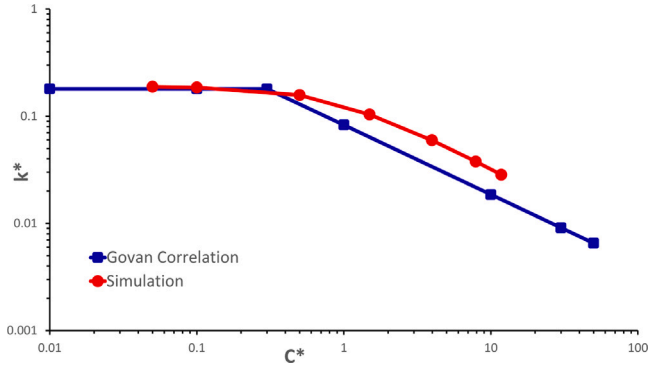


**Fig. 2.** Dimensionless deposition velocity plotted against the dimensionless particle concentration. Comparison of the simulation results with correlation from Govan (1990).

The factor $\phi$ which represents the deposition efficiency is a parameter which is unknown for this case and is taken as 0.2 as it provides a good agreement with experimental data. The deposition velocity is non-dimensionalized by the gas friction velocity. The relaxation time (T) for this plot is calculated by Eq. (17) and is non-dimensionalized as follows:

$$T^* = \frac{T v_{*G}^2}{\nu_G} \tag{33}$$

The next validation case considered was used from the work of Govan (1990) to demonstrate the effect of the droplet concentration on the deposition behavior. The gas mass flux was fixed at 100 $kg/m^2s$, and the liquid mass flux was varied from 5 to 1200 $kg/m^2s$. The geometry of the pipe used for this validation work was the same as the one used for the first case above. The change in concentration of the droplet volume fraction affects the droplet deposition behavior and the ability of the model to capture this is observed through this case. A droplet diameter of 20 μm was assumed for these simulations. Govan (1990) formulated a curve fit to match experimental data for deposition velocity versus particle concentration as follows,

$$k^* = \begin{cases} = 0.18 & if C^* < 0.3 \\ = 0.083(C^*)^{-0.65} & if C^* > 0.3 \end{cases} \tag{34}$$

The definition of the deposition velocity used for this plot is consistent with the definition used by Govan. The deposition efficiency $\phi$ is set to 0.5 as it is observed to give good agreement with the correlation of Govan as shown in Fig. 2. It is observed that the model captures the trend of the deposition velocity curve which changes slope as the concentration increases. However, the correlation of Govan predicts this change to be around $C^*$ value of 0.3, whereas the current simulation predicts this change at a higher concentration value of approximately 0.9. This leads to an overprediction of the deposition velocities for higher concentrations.

The next validation case is for testing the entrainment model in which a vertical pipe with a diameter of 9.5 mm and 4 m length is considered. Air is injected in the core, and a liquid film is injected from the bottom, along the walls of the pipe. The superficial velocity of the liquid is maintained at 0.6 m/s and that of the gas is varied from 60 to 140 m/s. The air strips off parts of the film in the form of droplets, and at the same time, the stripped droplets keep impacting and depositing on the wall. These two processes of stripping and deposition happen in tandem and eventually, the entrainment rate and deposition rate reach equilibrium as the two-phase flow flows through the pipe. In film experiments, the film is extracted at the end of the test section and the entrainment fraction is calculated as,

$$E = 1 - \frac{\dot{m}_{f\,out}}{\dot{m}_{f\,in}} \tag{35}$$

The gas Weber number is calculated as,

$$We_G = \frac{\rho_G v_{sG}^2 D_p}{\sigma} \left(\frac{\rho_L - \rho_G}{\rho_G}\right)^{1/3} \tag{36}$$

The plot of the entrainment fraction calculated from Eq. (35) is shown in Fig. 3. The results from the current work are compared with the correlations of Ishii and Mishima (1989) and Sawant et al. (2009). The entrainment fraction (E) was found to oscillate and so the results plotted are averaged over 1000 time steps. Similar to the work of Sawant et al. (2009), the initial steep increase in entrainment fraction with Weber number is clearly observed in Fig. 3. This initial region is followed by the transition region, and finally, as the Weber number increases futher, the entrainment fraction becomes independent of the Weber number, and achieves the limiting Entrainment fraction corresponding to the particular liquid Reynolds number. It is observed that the value of the limiting entrainment fraction predicted by the model is lower than that predicted by the two correlations. Overall, the trend suggests that the model underpredicts the amount of entrainment predicted by the two correlations, however, the slope and the trends are captured satisfactorily. In these simulations, both the entrainment and deposition models were active simultaneously in order to simulate the experimental conditions. The correlations are based on experimental data, and it is impossible in actual experiments to turn off one of these phenomena.

### 4.2. Turbulent film model validation

For validating the turbulent film model, the case of flow of a film over a horizontal flat plate was considered. A 2 m long flat plate is used, and the film was injected at a fixed velocity. The inlet thickness of the film was varied and the film flow is allowed to develop. Fig. 4 shows results for the developed film turbulence model and a laminar model based on parabolic velocity assumption plotted alongside the correlation of Kosky (1971), and the data of Asali et al. (1985).

The equation of Kosky (1971) and the data of Asali et al. (1985) show that between Reynolds numbers of 300 and 400, the flow behavior switches from laminar to turbulent, and the slope of line changes. It can be clearly seen that around the transition point, the turbulent film model accurately deviates from the laminar model predictions. An important point to note is that if a laminar model is assumed for the entire range of Reynolds numbers tested here, very large errors can be expected in the value of the predicted film thickness. For example,

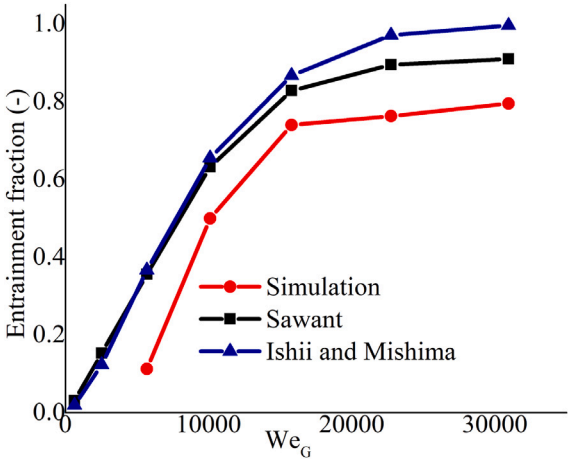


**Fig. 3.** Entrainment fraction plotted against the gas Weber number. Comparison of the simulation results with correlations from Ishii and Mishima (1989) and Sawant et al. (2009).

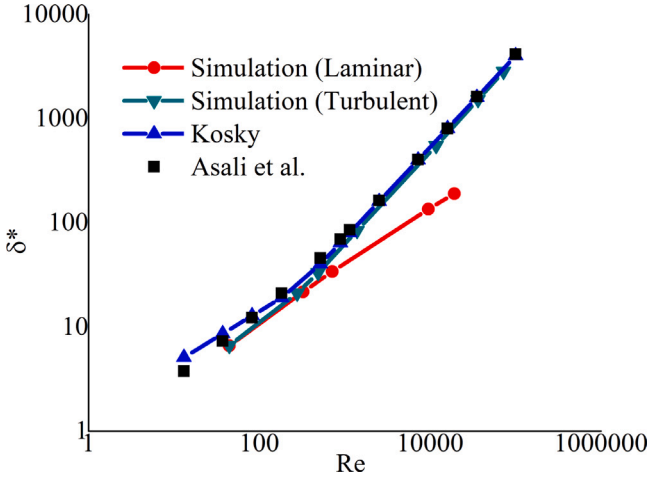


**Fig. 4.** Comparison of nondimensional film thickness predicted by the turbulent film model with the correlation of Kosky (1971) and experimental data of Asali et al. (1985).

if we consider the results for Re of 1000, there is approximated 50% difference between the predictions of $\delta^+$ by the laminar and turbulent models.

The second case was considered from the work of Karapantsios et al. (1989), in which a film was allowed to fall under the action of gravity in a pipe of inner diameter 50 mm. In the simulations, a pipe of length 3 m is considered, and the inlet thickness and velocity are varied to obtain a range of Reynolds Numbers. The flow is allowed to develop, and the average film thickness at the outlet of the pipe is plotted over a Re range of 509 to 13090. The results are plotted in Fig. 5. It is observed that, overall, the film turbulence model accurately captures the trends of the experimental data. The deviation between the laminar and turbulent predictions occurs around a Reynolds number between 700 and 800. After this point the results deviate significantly, and at a point of around $Re = 4500$, there is a 22% difference in film thickness predicted by the laminar and turbulent models.

### 4.3. Industrial application - Boiling water reactor (BWR)

One of the main industrial applications where annular flows appear are in BWR flow channels. As the liquid flows along the fuel rods, continuous impingement and entrainment take place which affect the film thickness, thereby affecting the dryout characteristics. Fig. 6 shows

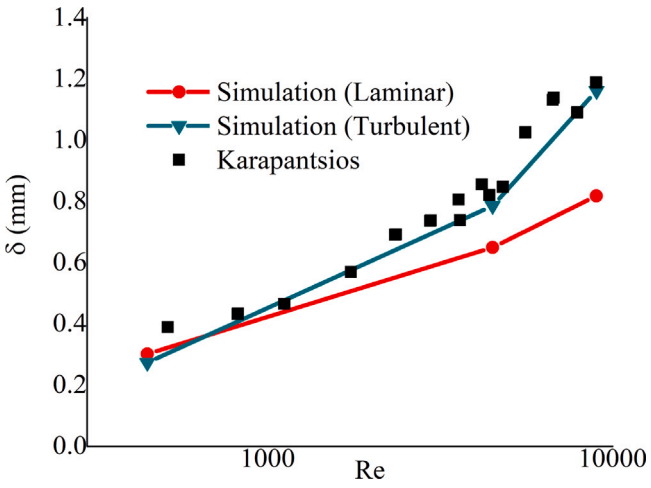


**Fig. 5.** Comparison of dimensional film thickness for falling film case with the experimental data of Karapantsios et al. (1989).

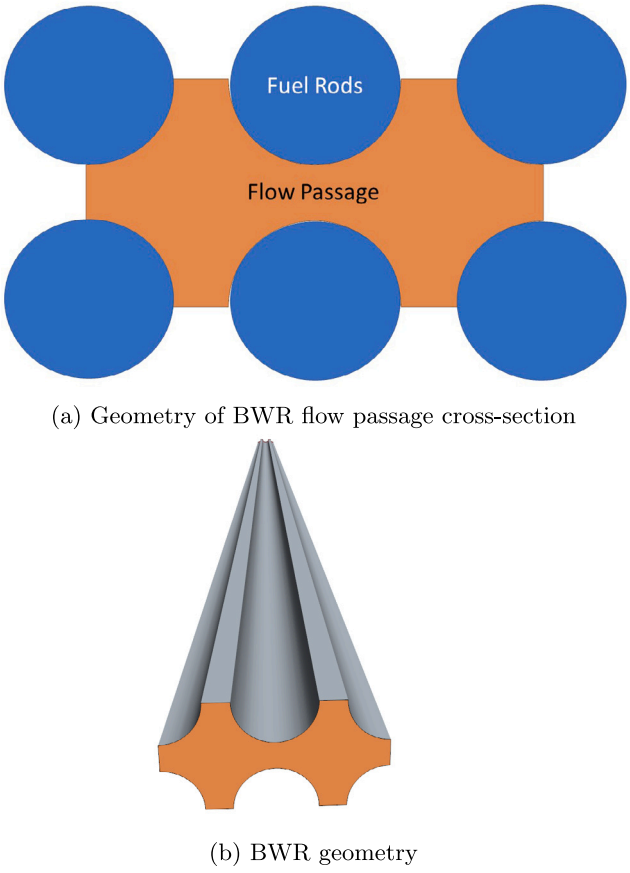


**Fig. 6.** BWR geometry used for demonstration of overall film modeling.

the geometry of the flow passage which is used in the simulations. The film is injected along the surface of the fuel rods. The superficial liquid velocity is 2 m/s and two cases with superficial gas velocities of 20 m/s and 40 m/s are run. The film is injected with a thickness of 0.3 mm. If these conditions are plotted on a multiphase flow regime map for vertical water flows, similar to the one shown in the work of Collignon et al. (2017), it can be seen that the conditions lie in the annular flow region.

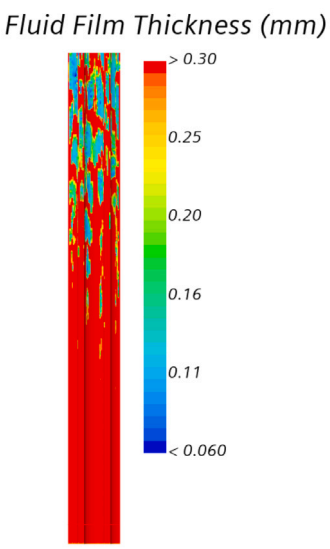


(a) Fluid Film Thickness contour plot

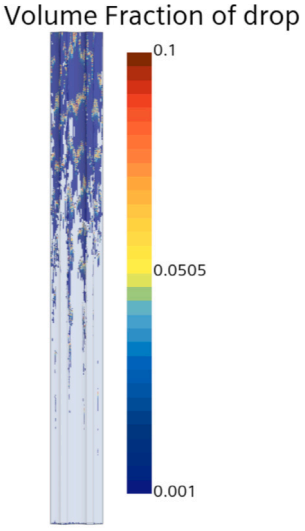


(b) Volume Fraction iso surface contour

**Fig. 7.** Contour plots for laminar case with $u_{sG}$ =20 m/s and $u_{sL}$ =2 m/s.

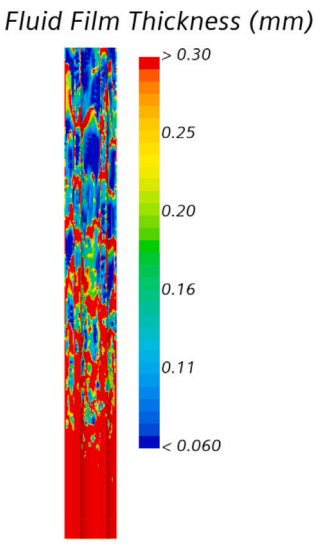


(a) Fluid Film Thickness contour plot


(b) Volume Fraction iso surface contour

**Fig. 8.** Contour plots for turbulent film case with $u_{sG}$ =20 m/s and $u_{sL}$ =2 m/s.

The Figs. 7 and 9 show the results for the laminar film flow through the BWR fuel rod assembly passage for the two different conditions specified above. Whereas Figs. 8 and 10 show the corresponding turbulent cases. The only difference between the two sets of cases is that the film is modeled either with laminar or turbulent model, all other model settings remain the same. It must be noted that the flow in the core is modeled as turbulent in both sets of cases.

As the film is injected from the bottom of the computational domain, the entrainment model predicts the onset of stripping based on the criteria of the unstable wavelength mentioned in Section 3.2.2 . As the stripping criteria is achieved, parts of the film strip off from the film, and flow in the form of droplets in gas. The stripping leads to the non-uniformity in the film thickness as seen in the contour plots. For the lower superficial gas velocity of 20 m/s, a large difference is observed between the laminar and turbulent solutions, with the turbulent case showing that the entrainment starts happening very close to the inlet itself. In the physical case, the onset of turbulence would be expected to make the surface of the film more unstable thereby leading to a higher degree of entrainment. This behavior is demonstrated qualitatively in the results of the 20 m/s case.

In the case with 40 m/s superficial velocity, both laminar and turbulent cases show stripping beginning from the entrance of the domain, and the results are qualitatively similar. As can be observed from Eq. (24), the unstable wavelength is a function of the slip velocity at the film surface $\Delta U$. As a result, in this case, the higher slip velocity leads to stripping occurring much earlier than the 20 m/s case.

In both these cases, the impingement model is also active and hence the process of stripping and impingement take place simultaneously as is expected in the experiment. The droplet volume fraction iso-surface plots show the stripped parts of the film flowing as droplets along with

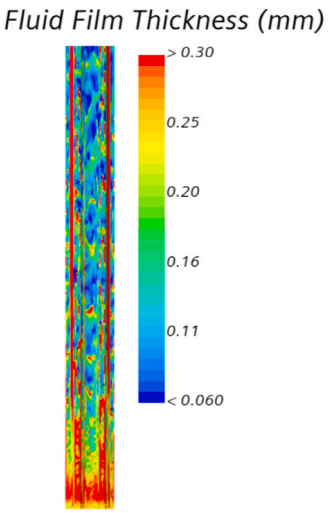


(a) Fluid Film Thickness contour plot

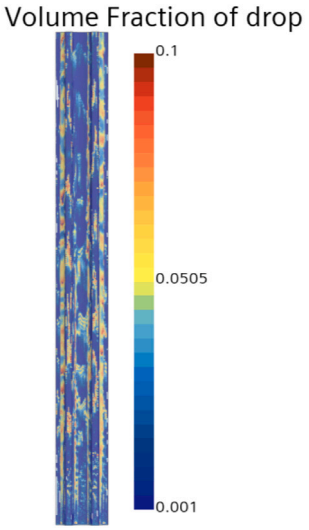


(b) Volume Fraction iso surface contour

**Fig. 9.** Contour plots for laminar case with $v_{sG}$ =40 m/s and $v_{sL}$ =2 m/s.

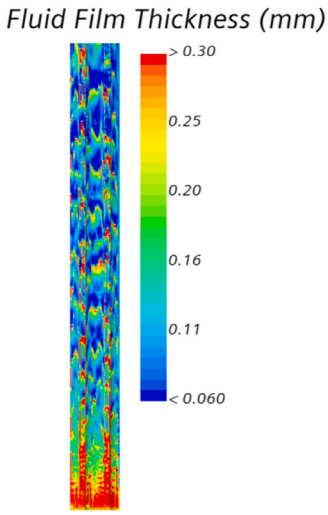


(a) Fluid Film Thickness contour plot

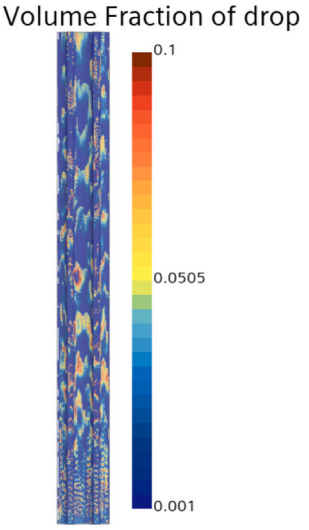


(b) Volume Fraction iso surface contour

**Fig. 10.** Contour plots for turbulent case with $v_{sG}$ =40 m/s and $v_{sL}$ =2 m/s.

the gas. From this plot also, it is clear that the higher superficial velocity case shows existence of droplets from the entry of the domain itself.

## 5. Conclusion

A model for simulating turbulence in liquid films based on the universal velocity profile is proposed. The model is implemented in the framework of Two-Fluid modeling of multiphase flows and coupled with different submodels to capture the effect of deposition and entrainment. The sub-model for droplet deposition is validated against available experimental data of Liu and Agarwal (1974) and the correlation of Govan (1990) for the change in Deposition Velocity with Particle Relaxation Time and Particle Concentration respectively. In order to validate the entrainment model, a vertical pipe is simulated with both deposition and entrainment models activated, and the results for the Entrainment Fraction are plotted with respect to the Weber number and compared with the correlations of Ishii and Mishima (1989) and Sawant et al. (2009). Next, the proposed turbulence model is validated against the correlation of Kosky (1971), and the data of Asali et al. (1985) for a film flowing on a horizontal surface. For a film falling under the effect of gravity, the experimental data of Karapantsios et al. (1989) was used for validation. Once the validity of the overall modeling technique was established, the next step was to apply the turbulent film model to industrial cases. For this purpose, flow over a 3D BWR fuel rod assembly was simulated. The different mechanisms like entrainment model and the impingement model work in tandem with the implemented turbulence model to predict behavior of the films in these industrial applications. The results clearly show that because of the higher film thickness predicted by the turbulence model, the entrainment behavior and thereby the overall flow behavior is drastically different between

the laminar and turbulent film cases. This demonstrates the importance of modeling turbulence in industrial cases like BWR.

Based on the available literature, it is believed that the current work is a novel attempt to develop a turbulent film model and combine it with different models for capturing mass exchanges in annular flows. As the liquid films in annular flows are very thin, and have a very wavy surface, it can be computationally expensive to resolve the films. As a result the simplified model presented in this work can be a good alternative to obtain results faster in large industrial scale cases.

Our future work will be focused on simulating heat transfer through the liquid film and on implementing a model for capturing film boiling and dry out.

## CRediT authorship contribution statement

**Kshitij Neroorkar:** Writing – review & editing, Writing – original draft, Investigation, Formal analysis. **Mohit P. Tandon:** Supervision, Investigation. **Dimitrios Papoulias:** Visualization, Validation.

## Declaration of competing interest

The authors declare that they have no known competing financial interests or personal relationships that could have appeared to influence the work reported in this paper.

## Data availability

No data was used for the research described in the article.

## References


Al-sarkhi, A., Sarica, C., 2013. Modeling of the droplet entrainment fraction in adiabatic gas-liquid annular flow. Multiph. Sci. Technol. 25 (1), 1–23.

Anglart, H., 2012. CFD modeling of annular two-phase flow and heat transfer. In: 12th International. July 12-16, Brussels, Belgium.

Anglart, H., Li, H., Niewinski, G., 2018. Mechanistic modelling of dryout and post-dryout heat transfer. Energy 161, 352–360.

Asali, J.C., Hanratty, T.J., Andreussi., P., 1985. Interfacial drag and film height for vertical annular flow. AIChE J. 31, 895–902.

Ashwood, A., Hogen, S.V., Rodarte, M., Kopplin, C., Rodriguez, D., Hurlburt, E., Shedd, T., 2015. A multiphase, micro-scale PIV measurement technique for liquid film velocity measurements in annular two-phase flow. Int. J. Multiph. Flow 68, 27–39.

Bai, C., Gosman, A.D., 1996. Mathematical modelling of wall films formed by impinging sprays. J. Engines 105, 782–796.

Calvert, S., Williams, B., 1955. Upward cocurrent annular flow of air and water in smooth tubes. AIChE J. 33, 885–891.

Camatte, P., Caré, I., Dumouchel, C., Ledoux, M., 1993. Modelisation of pulverisation systems: Some aspects of linear stability analysis. In: Instabilities in Multiphase Flows. Springer US, Boston, MA.

Caraghiaur, D., 2012. On Drops and Turbulence in Nuclear Fuel Assemblies of Boiling Water Reactors (Ph.D. thesis). KTH School of Engineering Sciences.

Caraghiaur, D., Anglart, H., 2008. Langrangian particle tracking as a tool for deposition modeling in annular flow. In: Proceedings of the 17th International Conference on Nuclear Engineering (ICONE17). July 12-16, Brussels, Belgium.

Cioncolini, A., Thome, J., 2010. Prediction of the entrained liquid fraction in vertical annular gas-liquid two-phase flow. Int. J. Multiph. Flow 36, 293–302.

Cioncolini, A., Thome, J., Lombardi, C., 2009. Algebraic turbulence modeling in adiabatic gas-liquid annular two-phase flow. Int. J. Multiph. Flow 35, 580–596.

Collignon, M., Mazzini, A., Schmid, D.W., Lupi, M., 2017. Modelling fluid flow in active clastic piercements: Challenges and approaches. Mar. Pet. Geol. 90, 157–172.

Damsohn, M., 2011. Liquid Films and Droplet Deposition in a BWR Fuel Element (Ph.D. thesis). ETH Zurich.

Dukler, A.E., 1959. Fluid mechanics and heat transfer in falling film systems. In: ASME-AIChE 3rd National Heat Transfer Conference.

Foucart, H., 1998. Modélisation tridimensionnelle des films liquides pariétaux dans les moteurs à combustion interne (Ph.D. thesis). University of Rouen Normandy.

Friedman, S.J., Miller, C., 1941. Liquid film in the Viscous Flow Region. Ind. Eng. Chem. 78.

Govan, A., 1990. Modelling of Vertical Annular Flows And Dispersed Two-Phase Flows (Ph.D. thesis). Imperial College, University of London, Chapter 3.

Hewitt, G., Govan, A., 1990. Phenomenological modelling of non-equilibrium flows with phase change. Int. J. Heat Mass Transfer 33 (2), 229–242.

Hewitt, G., Hall-Taylor, N., 1970. Annular Two-Phase Flow. Pergamon Press, Section 8.7.2.

Hewitt, G., Lacey, P., 1965. The breakdown of the liquid film in annular two-phase flow. Int. J. Heat Mass Transfer 8 (5), 781–791.

Hinze, J., 1975. Turbulence. McGraw-Hill, Incl.

Holowach, M., 2002. A Physical Model For Predicting Droplet Entrainment In Transient Two-Phase Fluid Flow And Heat Transfer Systems Analysis Computer Codes (Ph.D. thesis). Pennsylvanie State University.

Ishii, M., Mishima, K., 1989. Droplet entrainment correlation in annular two-phase flow. Int. J. Heat Mass Transf. 32 (10), 1835–1846.

Joseph, D., Bannwart, A., Liu, Y., 1996. Stability of annular flow and slugging. Int. J. Multiph. Flow 22 (6), 1247–1254.

Karapantsios, T.D., Paras, S.V., Karabelas, A.J., 1989. Statistical characteristics of free falling films at high Reynolds numbers. Int. J. Multiph. Flow 15, 1–21.

Kosky, P., 1971. Thin-liquid films under simultaneous shear and gravity forces. Int. J. Heat Mass Transfer 14, 1220–1224.

Ledoux, M., 1993. Modélisation des sprays. In: Cours de DEA.

Lefebvre, A., McDonell, V., 2017. Atomization and Sprays. CRC Press.

Li, H., Anglart, H., 2015. CFD model of diabatic annular two-phase flow using the Eulerian–Lagrangian approach. Ann. Nucl. Energy 77, 415–424.

Liu, B., Agarwal, J., 1974. Experimental observation of aerosol deposition in turbulent flow. Aerosol Sci. 5, 145–155.

Liu, L., Bai, B., 2017. Generalization of droplet entrainment rate correlation for annular flow considering disturbance wave properties. Chem. Eng. Sci. 164, 279–291.

Maroteaux, F., Llory, D., Coz, J.-F.L., Habchi, C., 2002. Liquid film atomization on wall edges—Separation criterion and droplets formation model. J. Fluids Eng. 124 (3), 565–575.

McPherson, G., 1970. Axial stability of the dry patch formed in dryout of a two-phase annular flow. Int. J. Heat Mass Transfer 13 (7), 1133–1152.

Meredith, K.V., Heather, A., de Vries, J., Xin, Y., 2011. A numerical model for partially-wetted flow of thin liquid films. Comput. Methods Multiphase Flow VI 70, 239–250.

Mori, S., Fukano, T., 2003. Influence of a flow obstacle on the occurrence of burnout in boiling two-phase upward flow within a vertical annular channel. Nucl. Eng. Des. 225 (1), 49–63.

Neroorkar, K., Tandon, M., 2022. Effect of turbulence on modeling of liquid films. In: The 19th International Topical Meeting on Nuclear Reactor Thermal Hydraulics (NURETH-19) Log Nr.: 34174 Brussels, Belgium, March 6 - 11, 2022.

Okawa, T., Kotani, A., Kataoka, I., Naito, M., 2003. Prediction of critical heat flux in annular flow using a film flow model. J. Nucl. Sci. Technol. 40 (6), 388–396.

Oliemans, R., Pots, B., Trompe, N., 1986. Modeling of annular dispersed two-phase flow in vertical pipes. Int. J. Multiph. Flow 12, 711–732.

Paleev, I., Filippovich, B., 1966. Phenomena of liquid transfer in two-phase dispersed annular flow. J. Heat Mass Transf. 9, 1089–1093.

Sawant, P., Ishii, M., Mori, M., 2009. Prediction of amount of entrained droplets in vertical annular two-phase flow. Int. J. Heat Fluid Flow 30, 715–728.

Tandon, M., Khanolkar, A., Splawski, A., Lo, S., 2013. Validation of numerical simulations of gas-liquid systems in a vertical pipe. In: Proceedings of 8th International Conference in Multiphase Flow. ICMF, Jeju, Korea.

Utsuno, H., Kaminaga, F., 1998. Prediction of liquid film dryout in two-phase annular-mist flow in a uniformly heated narrow tube development of analytical method under BWR conditions. J. Nucl. Sci. Technol. 35, 643–653.

Vasallo, P., 1999. Near wall structure in vertical air-water annular flows. Int. J. Multiph. Flow 25, 459–476.

Vikhansky, A., Splawski, A., 2015. Adaptive multiply size group method for CFD-population balance modelling of polydisperse flows. Can. J. Chem. Eng. 93 (8), 1327–1334.

Xue, Y., Stewart, C., Kelly, D., Campbell, D., Gormley, M., 2022. Two-phase annular flow in vertical pipes: A critical review of current research techniques and progress. Water 14 (21).

Young, B., Leeming, A., 1997. A theory of particle deposition in turbulent pipe flow. J. Fluid Mech. 340, 129–159.

Zaichik, L., Alipchenkov, V., Sinaisk, E., 2008. Particles in Turbulent Flows. WILEY-VCH Verlag Gmb&Co.